Positive and negative impacts of interfacial hydrogen bonds on photocatalytic hydrogen evolution

Zhongqiu Lin[1,2], Hikaru Saito[1], Hiromasa Sato[1] and Toshiki Sugimoto[1,2,*]

[1]Department of Materials Molecular Science, Institute for Molecular Science, Okazaki, Aichi 444-8585, Japan

[2]Graduate Institute for Advanced Studies, SOKENDAI, Okazaki, Aichi 444-8585, Japan

ABSTRACT: Understanding the behavior of water molecules at solid–liquid interfaces is crucial for various applications such as photocatalytic water splitting, a key technology for sustainable fuel production and chemical transformations. Despite extensive studies conducted in the past, the impact of microscopic structure of interfacial water molecules on photocatalytic reactivity has not been directly examined. In this study, using real-time mass spectrometry and Fourier-transform infrared spectroscopy, we demonstrated the crucial role of hydrogen bond (H-bond) networks on the photocatalytic hydrogen evolution in thickness-controlled water adsorption layers on various TiO_2 photocatalysts. Under controlled water vapor environments with a relative humidity (RH) below 70%, we observed a monotonic increase in the H_2 formation rate with increasing RH, indicating that reactive water molecules were present not only in the first adsorbed layer but also in several overlying layers. In contrast, at RH > 70%, when more than three water layers covered the catalyst surface, the H_2 formation rate turned to decrease dramatically because of the structural rearrangement and hardening of the interfacial H-bond network induced during further water adsorption. This unique many-body effect of interfacial water was consistently observed for various TiO_2 particles with different crystalline structures, including brookite, anatase, and a mixture of anatase and rutile. Our results demonstrated that depositing several water layers in a water vapor environment with RH ~70% is optimal for photocatalytic hydrogen evolution rather than liquid-phase reaction conditions in aqueous solutions. This study provides molecular-level insights for designing interfacial water conditions to enhance photocatalytic performance.

Introduction

The photocatalytic hydrogen evolution from water is a key technology for achieving sustainable and environmentally friendly hydrogen production. Since its initial discovery by Honda and Fujishima in 1972, numerous studies[1–4] have been conducted to achieve a comprehensive understanding of this process and expand the scope of its practical applications. The photocatalytic process involves three fundamental steps: (1) the generation of photoinduced carriers via light absorption, (2) separation and diffusion of these carriers, and (3) transfer of electrons and holes between the interfacial molecules and photocatalyst surface, leading to the subsequent redox reactions. The first two steps are predominantly governed by the bulk semiconducting properties of the photocatalyst.[1,5] In contrast, the physicochemical properties of the interfacial water molecules are critical in the final step.[6–9]

A key aspect of optimizing the surface reaction environment is gaining detailed insights into the interfacial hydrogen bond (H-bond) networks.[7,10–12] The interfacial H-bonds are characterized by the interactions between the adsorbed water molecules and photocatalyst surface, as well as by the intermolecular interactions among the adsorbed water molecules. On metal oxide surfaces with few adsorbed H_2O molecules, these H_2O molecules predominantly forms H-bonds with the surface oxygen anions.[12,13] As the amount of H_2O molecules increases, H-bonds are rapidly generated owing to these intermolecular interactions, leading to the development of intricate H-bond networks.[11,14–16] The formation and impact of H-bonds depend on the photocatalyst surface structure, including its local surface morphology and adsorption sites.[12] In this context, the effects of H-bonding on the transfer of photoinduced holes and H_2O dissociation have been extensively investigated with various analytical approaches.[12,17–20] Despite these studies, however, the direct relationship between the microscopic structure of interfacial water molecules and overall hydrogen evolution remains unestablished.

In this study, we successfully demonstrated the impact of interfacial H-bond networks on the H_2 formation rate by combining real-time mass spectrometry with infrared (IR) absorption spectroscopy. Although IR spectroscopy is a powerful tool for investigating the H-bond structure,[21,22] the abundance of bulk water molecules in solution has impeded the observation of interfacial water molecules on

photocatalyst surfaces. To overcome this challenge, we carried out our experiments in controlled water vapor environments and systematically varied the thickness of the adsorbed water layer in the angstrom to nanometer range. For various Pt-loaded TiO2 photocatalysts with different crystalline structures, we showed that the H_2 formation rate almost linearly increased with the adsorbed water amount up to three layers. However, when more than three water layers covered the catalyst surface, the H_2 formation rate turned to decrease dramatically due to the structural rearrangement and hardening of the interfacial H-bond networks. These findings indicate that depositing several water layers in a water vapor environment is optimal for photocatalytic hydrogen evolution in contrast to the commonly used liquid-phase reaction conditions in aqueous solutions where catalyst surfaces are covered with infinitely thick water layers.

Experimental methods

Photocatalyst preparation

Commercial TiO_2 photocatalysts with different crystalline structures were used in this study. They included brookite (TIO19PB; Kojundo Chemical Lab.), anatase (ST01; Ishihara Sangyo), and a mixture of anatase and rutile (P25; Nippon Aerosil). To enhance their photocatalytic performance, they were coated with a Pt cocatalyst using a photodeposition method. To prepare 1 wt.% Pt/TiO_2, 0.125 mL of a H_2PtCl_6•$6H_2O$ solution (Sigma–Aldrich, 8%) and 4 mL of ethanol (Fujifilm Wako Chemical, concentration: >99.5%) were added to 100 mL of distilled water, and 0.5 g of TiO_2 powder was dispersed in the prepared solution. The resultant slurry was irradiated with ultraviolet (UV) light for 1 h using a Xe lamp (UXL-500SX; Ushio). After irradiation, the TiO_2 slurry was centrifuged and dried for 20 h at 90 °C in static air. The prepared Pt/TiO_2 samples were used for photocatalytic water splitting and IR absorption spectroscopy.

Evaluation of photocatalytic activity for H_2O splitting

The photocatalytic performances of the prepared samples were assessed using a stainless-steel batch reactor. A photocatalyst sample was loaded into the reaction chamber and evacuated to ultra-high vacuum (UHV) using a turbomolecular pump. Liquid water (H_2O and D_2O) was predegassed in a UHV gas line by performing freeze–pump–thaw cycles, after which water vapor was introduced into the UHV chamber. Next, the sample was irradiated with a light-emitting diode at a wavelength of 365 nm and intensity of ~15 mW cm^{-2} through a CaF_2 window. The sample temperature was measured using a chromel–alumel (type K) thermocouple directly inserted into the powdered samples, which allowed accurate determination of the relative humidity (RH) of the water-adsorbed catalyst particles. During UV irradiation, the sample temperature increased from room temperature (24 °C) to 27 °C. Reaction products were quantified using a quadrupole mass spectrometer (QME220; Pfeiffer Vacuum)

Diffuse reflectance infrared Fourier transform spectroscopy of adsorbed H_2O species

To examine the adsorption of water molecules on the photocatalyst surface, diffuse reflectance infrared Fourier transform (DRIFT) spectroscopy was performed using a Fourier-transform infrared spectrometer (IRTracer-100; Shimadzu Corp.), which was attached to the reactor utilized for the photocatalytic activity evaluation. DRIFT spectra were obtained using a mercury–cadmium–telluride detector at a resolution of 4 cm^{-1}. DRIFT measurements were performed without UV irradiation at room temperature. The background spectrum of silicon powder was employed to estimate the relative reflectance, and the IR intensity of the adsorbed water species was calculated using the Kubelka–Munk function. Adsorbed water species were quantified based on their peak areas in the H_2O bending mode. The dependence of the water vapor pressure on the peak areas is described by the Brunauer–Emmet–Teller adsorption isotherm equation, as described in Supporting Information.

Results and discussion

Initially, the water splitting activity was investigated under various water vapor conditions. Fig. 1a shows the H_2 evolution during the photocatalytic water splitting using the brookite TiO_2 photocatalyst. In the low-pressure regions, the H_2 formation rate increases with the water vapor pressure (left in Fig. 1a); however, it decreases drastically at water vapor pressures higher than ~2400 Pa (right in Fig. 1a). Notably, the H_2 formation yield linearly increases with the UV irradiation time at all water vapor pressures, indicating that the reverse reactions[23,24] were negligible under our experimental conditions. Therefore, the variations in the H_2 formation rate in Fig. 1a are not attributed to reverse reactions.[23,24] The temperature of the UV-irradiated photocatalyst samples was not equal to the room temperature due to thermal heating induced by the UV light. Therefore, the H_2 formation rate is plotted as a function of RH with the results presented in Fig. 1b (filled green circles). Here, RH is defined as P/P_0, where P represents the water vapor pressure, and P_0 is the saturated water vapor pressure at the photocatalyst temperature during UV irradiation. The H_2 formation rate first monotonically increases up to ~70% RH and then significantly decreases above 70% RH.

A similar RH-dependent behavior was observed in the D_2 evolution via D_2O splitting (Fig. 1b, filled pink circles), conforming that the evolved hydrogen gas species originated from the adsorbed water molecules in the vapor environment and not from surface-adsorbed contaminants.[3,25] Notably, the rate of H_2 formation from H_2O is three times higher than that of D_2 from D_2O (Fig. 1b). This kinetic isotope effect is consistent with the results of previous studies,[26] indicating that the cleavage of the O–H (or O–D) bond is the rate-determining step in the water splitting process.[18,26]

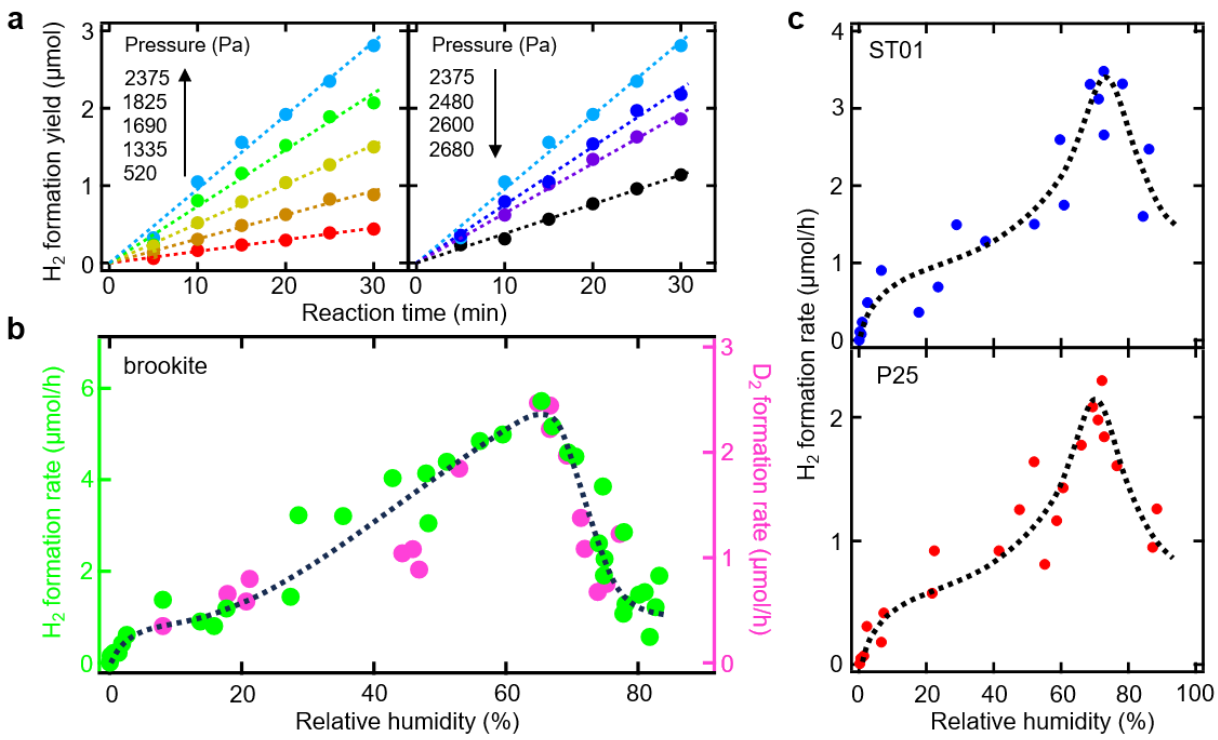

Figure 1. Photocatalytic performance analysis. (a) H_2 evolution over the brookite TiO_2 photocatalyst plotted as a function of the irradiation time at various H_2O pressures. (b) Formation rates of H_2 (filled green circles) and D_2 (filled pink circles) over the brookite TiO_2 photocatalyst plotted as functions of RH for H_2O and D_2O vapors, respectively. (c) H_2 formation rates over the ST01 (top) and P25 (bottom) photocatalysts plotted as functions of RH.

Remarkably, the ST01 (anatase) and P25 (mixture of anatase and rutile) TiO_2 photocatalysts exhibited similar responses to RH variation (Fig. 1c), mirroring the behavior of brookite TiO_2. For these photocatalysts, the H_2 formation rates initially increase monotonically up to ~70% RH and then decrease above ~70% RH. Consequently, the observed positive and negative impacts of RH variation on the H_2 formation rate are universal characteristics of TiO_2 regardless of its crystalline structure. During these experiments, no oxygen evolution was observed, even though H_2 (D_2) evolution from water molecules was observed for H_2O (D_2O) vapor environments (Fig. 1b). Previous studies suggest that water species activated by photoinduced holes tend to partially oxidize, forming peroxide species such as H_2O_2,[27–29] rather than being completely oxidized into oxygen.

It is noteworthy that some researchers reported a monotonically increasing relationship between the H_2 formation rate and RH under water vapor conditions even at high RH values (>70%).[30,31] However, in these studies, RH was determined based on the temperature inside the reaction chamber without accounting for the inevitable increase in the photocatalyst temperature caused by photoirradiation. As a result, RH was likely overestimated, leading to an evaluation of water splitting activities at actual RH values lower than expected.[30,31] We believe that the RH dependencies reported in these previous studies are consistent with the results obtained in the low RH region in the present work (see Supporting Information for more detail).

To gain molecular-level insights into the impact of RH variation on photocatalytic performance, DRIFT spectroscopy was systematically conducted for the adsorbed water species under various water vapor pressures. Typical DRIFT spectra of brookite TiO_2 (Fig. 2a) exhibit two prominent peaks at 1650 and ~3300 cm^{-1}, which are attributed to the H_2O bending and O–H stretching bands, respectively. The area of these bands increases with increasing water vapor pressure. The bending band area is almost linearly proportional to the amount of adsorbed water molecules,[11,32] as the oscillator strength of the bending mode remains nearly unchanged, regardless of the surrounding H-bonding environment. Therefore, we plotted the bending area as a function of RH and estimated the amount of adsorbed water by fitting the obtained graph with a Brunauer–Emmett–Teller (BET) adsorption isotherm[11,32] (Fig. 2b; see Supporting Information for more details). By analyzing the adsorption isotherm, we derived the relationship between the H_2 formation rate and the amount of adsorbed water molecules (θ). As shown in Fig. 2c, the H_2 formation rate of brookite sample initially increases almost linearly with θ up to 3 ML of adsorbed water, then decreases dramatically from 3 to 5 ML, and finally approaches saturation at $\theta \geq 5$ ML, with the saturation value approximating that at ~1 ML. For the ST01 and P25 samples, the adsorption isotherms (Fig. S1) and the variations in H_2 formation rates with θ (Fig. S2) are similar to those of the brookite sample. These consistent experimental results of various TiO_2 photocatalysts with different crystalline structures clearly indicate participation in the photocatalytic processes not only from

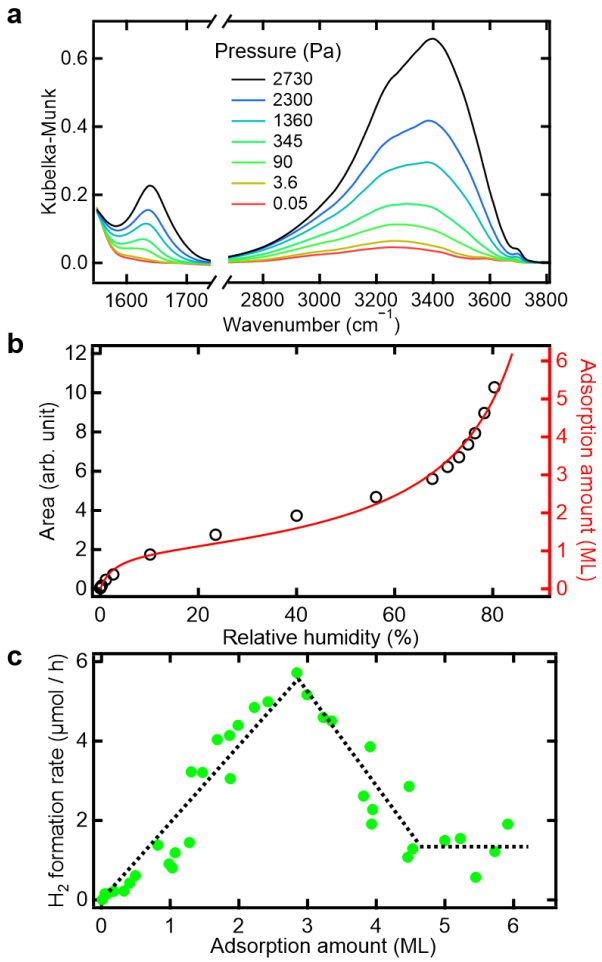

Figure 2. (a) DRIFT spectra of brookite TiO_2 recorded at various water vapor pressures. (b) Integrated areas of the bending bands (open black circles) and numbers of adsorbed H_2O layers determined from the adsorption isotherms (red line) at various RH values. (c) H_2 formation rate versus the number of adsorbed H_2O layers.

the water species interacting with the photocatalyst surfaces (first layer), but also from those in a few overlayers. that not only the water species. Furthermore, all these samples exhibited their maximum hydrogen formation rate at θ~3 ML of adsorbed water, with the rate decreasing as θ increases (Figs. 2c and S2), suggesting that a water vapor environment with an optimal amount of adsorption provides a more suitable platform for photocatalytic hydrogen evolution than the liquid–phase environment, which involves an infinite number of water overlayers.

Figs. 3, 4, and S3 illustrate the DRIFT spectra of the O–H stretching bands, highlighting the influence of RH variation on the H-bonding network of adsorbed water molecules. The O–H stretching frequency is generally used as an indicator of the strength of H-bonding networks; the lower wavenumber of the O–H stretching peak indicates stronger (more rigid) H-bonds.[12,33,34] Fig. 3 shows the normalized difference spectra at various RH conditions for the brookite sample, while the spectra for ST01 and P25 samples are displayed in Fig. S3. According to Fig. 3, the peak position of the O–H stretching band in the difference

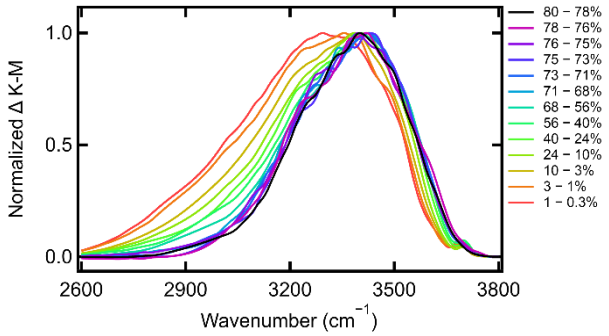

Figure 3. Normalized difference spectra obtained by subtracting the DRIFT spectra of the O–H stretching bands between two different RH levels of brookite TiO_2.

DRIFT spectra shifts from ~3300 to ~3400 cm^{-1} with increasing RH to ~70%. At RH < 10%, the adsorbed water molecules within the first layer formed stronger H-bonds with the TiO_2 surface as compared with those of liquid bulk water. The adsorption energy of this directly adsorbed layer estimated from the adsorption isotherm, was 53 kJ/mol, exceeding the condensation energy (H-bonding strength) of liquid water (44 kJ/mol, Table S2). At RH values above ~10%, water molecules began to adsorb on the second layer and form intermolecular H-bonds with the first layer. Above ~70% RH, H-bond networks were also formed with water molecules in the third layer and above. The difference DRIFT spectrum of the adsorbed water layers above ~70% (Fig. 3) closely resembles the IR spectrum of bulk liquid water.[22,35] Remarkably, at ~70% RH, where liquid-like water characteristics emerged, the photocatalytic hydrogen formation rates began to decrease (Fig. 1). A similar trend was also observed in ST01 and P25 samples (Figs. 1 and S3).

Based on these results, we categorized the adsorbed water into two types: interfacial water and liquid-like water. We then deconvoluted the DRIFT spectra into these two components. The typical result of the spectral decomposition for water adsorbed on the brookite sample is shown in Fig. 4a. Detailed methodology and comprehensive spectral decomposition data at various RH values are available in the Supporting Information (Sec. 5). Fig. 4b shows the integrated areas of the total O–H stretching band, decomposed interfacial water component, and liquid-like water component at various RH for the brookite sample. The same analysis was conducted for the ST01 and P25 samples (Figs. S5 and S6) and results similar to Fig. 4b were obtained (Fig. S7). Assuming that the thickness of one water layer is approximately 0.3 nm,[36,37] it can be concluded that properties of the adsorbed water molecules located ~1 nm away from the photocatalyst surface are similar to those of bulk liquid water, corroborating previous theoretical predictions.[14,38]

To examine the effect of the liquid-like water adsorption in the overlayers on the H-bond network structure of interfacial water and photocatalytic activity, we focused on the spectral variation of the interfacial water component with RH. Fig. 4c shows a two-dimensional plot of the peak-normalized spectra recorded for the O–H stretching band

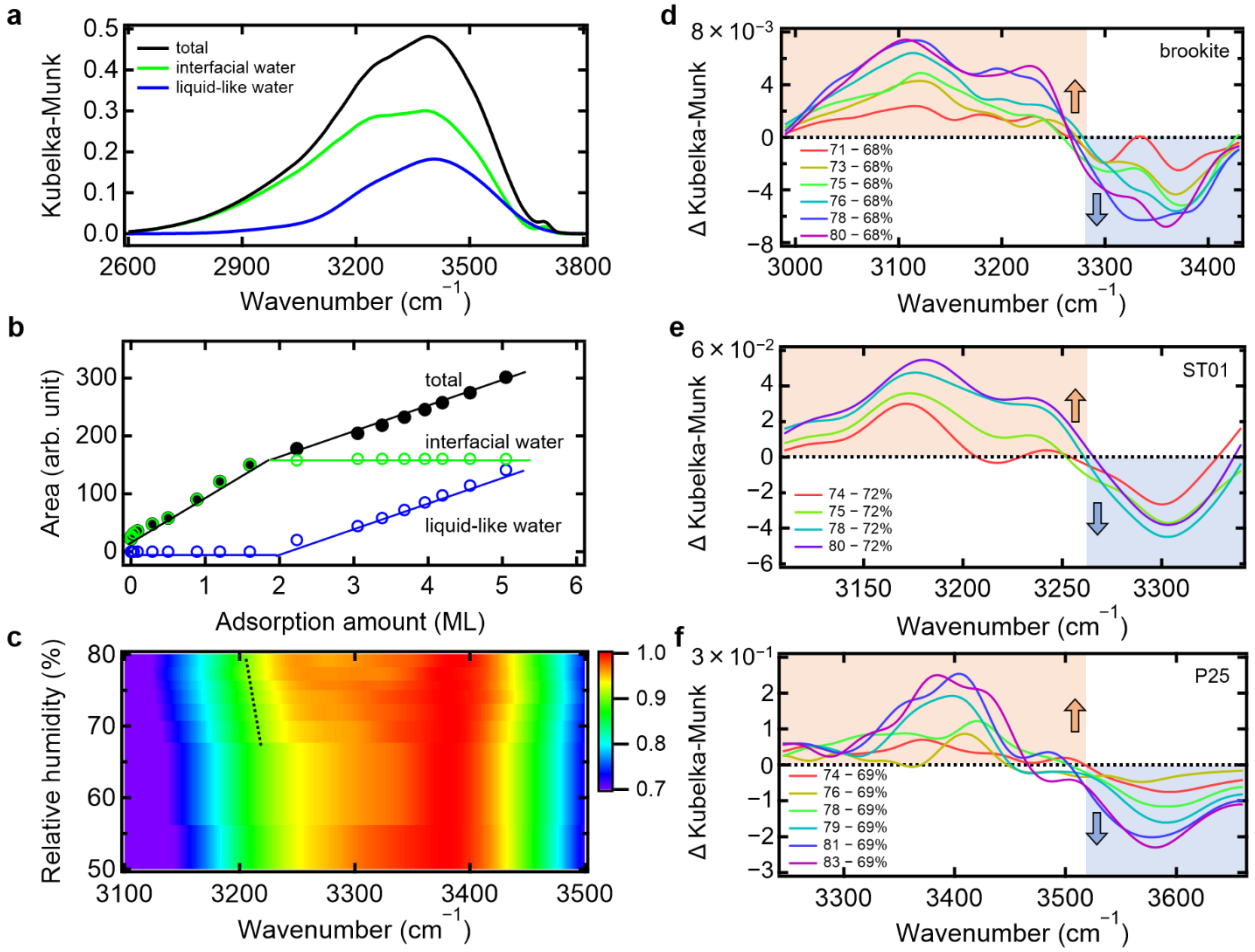

Figure 4. Impact of water adsorption on interfacial H-bonds. (a) Typical DRIFT spectrum of the adsorbed water on brookite TiO_2 at 73% RH, decomposed into interfacial water (open green circles) and liquid-like water (open black circles). (b) Integrated area of the O–H stretching bands for all adsorbed water on brookite TiO_2 (filled black circles), plotted as a function of the number of adsorbed water layers. It also includes the integrated area of interfacial water (open green circles) and liquid-like water overlayer (open blue circles). The solid lines are added for visual clarity. (c) Two-dimensional plot of the peak-normalized O–H stretching bands of the interfacial water component on brookite TiO_2 at various RH values, which are derived via spectral decomposition (see Sec.5. in Supporting Information for details). The dashed line serves as a visual guide to the spectral red shift. (d–f) Changes in the O–H stretching bands of the interfacial water component with the adsorption of liquid-like water overlayers at high RH values (>70%), obtained by subtracting the spectrum of the interfacial water component recorded at ~70% RH for brookite (d), ST01 (e), and P25 (f) TiO_2 samples.

of the interfacial water component on brookite TiO_2 at various RH values. The spectral shape of the interfacial water component is invariable at RH values between 50–70% ($2 \leq \theta \leq 3$ ML). However, it begins to change gradually above 70% RH ($\theta > 3$ ML), as illustrated by the dashed line in Fig. 4c, indicating that the H-bond networks of interfacial water with a sub-nanometer thickness were continuously modulated/rearranged due to the increase in the number of liquid-like bulky water overlayers. For a more detailed analysis, we examined the spectral changes occurring at RH > 70% (Fig. 4d), the point where H_2 formation rate reached its maximum and then began to decrease. For the brookite TiO_2 sample, distinct positive and negative peaks appear at ~3150 and ~3350 cm^{-1} respectively, indicating a red shift in the interfacial water spectra with increasing RH above ~70%. Fig. 4e and f demonstrate similar bipolar spectral changes, characterized by a red shift in the interfacial water component, for both ST01 and P25 samples above ~70% RH. Despite the different variations in the O–H stretching frequency among these TiO_2 samples, the red shift caused by the adsorption of the liquid-like water overlayers was consistently observed. These commonly observed results on various TiO_2 samples strongly indicate that the formation of the liquid-like water overlayer strengthened and hardened the interfacial H-bonds, possibly due to the cooperative many-body effects characteristic of H-bonding networks of water.[39–41]

The spectroscopic results (Figs. 3 and 4) provide a clear explanation for the positive and negative impacts of RH variations on photocatalytic activity (Fig. 1). As previously discussed, the rate-determining step in water splitting is the O–H bond cleavage of an adsorbed water molecule via hole oxidation.[18,26] This cleavage process typically involves a localized proton transfer between neighboring water molecules.[42,43] The H_2 formation rate increased almost linearly with increasing θ and reached its maximum at ~3 ML (~70% RH) of adsorbed water as shown in Fig. 2c and S2.

This indicates that hole transfer was not restricted to the first water layer, but extended to several adsorbed water layers (Fig. S8),[44] leading to an increase in reactant water molecules. However, above 3 ML of adsorbed water, the liquid-like water overlayers formed, resulting in hardening and strengthening of interfacial H-bonding networks, as characterized by the red shift in the O–H stretching band (Fig. 4). Therefore, the decrease in the H_2 formation rate (Fig. 1) can be directly related to alterations in the structure and dynamics of the interfacial H-bond networks of water.

Because O–H cleavage is a proton-coupled hole transfer process, the reorientation of photoactivated water species and adjacent water molecules is crucial for promoting the rate-determining step according to the Marcus theory.[45,46] In rigid H-bond networks, water molecules bind strongly to each other and retain an ordered structure.[47] Consequently, their reorganization dynamics may be limited,[48,49] making proton-coupled hole transfer less favorable. Indeed, previous studies suggested that a larger coverage of water molecules can suppress hole transfer by forming strong H-bond networks between H_2O molecules.[20] Our experiments combining mass spectrometry and IR spectroscopy on various TiO_2 samples demonstrated that the adsorption of liquid-like water overlayers not only rearranged the interfacial H-bond networks (Fig. 4) but also deteriorated the photocatalytic performance (Fig. 1). Consequently, a higher reaction activity can be achieved under water vapor conditions rather than in aqueous reaction environments.

Note that this study highlights the commonly observed phenomena induced by water adsorption on various TiO_2 photocatalysts. However, as discussed previously, the reaction activity, reaction dynamics, and structures of interfacial water are also influenced by the physical characteristics of photocatalysts, such as particle size, crystalline structure, surface morphology, and facets.[7,12,50–52] Indeed, our results showed that there are slight differences in the reaction activities (Fig. 1) and interfacial H-bond structures (Fig. 4) among different TiO_2 samples. Detailed quantitative insights into these sample-dependent characteristics will be provided in our forthcoming paper.

Conclusion

By precisely controlling the amount of adsorbed water molecules and combining real-time mass spectrometry and IR spectroscopy, we systematically investigated the optimal conditions for photocatalytic water splitting on various Pt-loaded TiO_2 catalysts with different crystalline structures. Under the low relative humidity conditions (RH < 70%), the H_2 formation rate increased monotonically with increasing RH, demonstrating that the involvement of adsorbed water molecules in the water-splitting process is not restricted to a single monolayer but extends to several overlying water layers. In contrast, as the thickness of the adsorbed water layer further increased, the interfacial H-bond networks became more rigid due to the many-body H-bond cooperative effects, which inhibited hydrogen evolution. Our findings provide novel molecular-level insights into many-body interfacial phenomena between water molecules and present essential concepts for optimally engineering interfacial water, leading to more efficient and sustainable hydrogen production beyond the current mainstream framework of catalysts material engineering[1–4].

ASSOCIATED CONTENT

Supporting Information. Influence of surface temperature on relative humidity; Analysis of adsorption isotherm; H_2 formation rate dependence on the water layer thickness; The spectra of water molecules adsorbed on anatase and P25 TiO_2; Decomposition of DRIFT spectral component into interfacial and liquid-like water; Schematic of impact of water adsorption. This material is available free of charge via the Internet at http://pubs.acs.org.

AUTHOR INFORMATION

Corresponding Author

Toshiki Sugimoto* – Department of Materials Molecular Science, Institute for Molecular Science, Okazaki, Aichi 444-8585, Japan; Graduate Institute for Advanced Studies, SOKENDAI, Okazaki, Aichi 444-8585, Japan;
ORCID: https://orcid.org/0000-0003-3453-6009
Email: toshiki-sugimoto@ims.ac.jp

Authors

Zhongqiu Lin – Department of Materials Molecular Science, Institute for Molecular Science, Okazaki, Aichi 444-8585, Japan; Graduate Institute for Advanced Studies, SOKENDAI, Okazaki, Aichi 444-8585, Japan;
ORCID: https://orcid.org/0000-0002-7602-1073
Hikaru Saito – Department of Materials Molecular Science, Institute for Molecular Science, Okazaki, Aichi 444-8585, Japan;
ORCID: https://orcid.org/0000-0002-2845-5053
Hiromasa Sato – Department of Materials Molecular Science, Institute for Molecular Science, Okazaki, Aichi 444-8585, Japan;
ORCDI: https://orcid.org/0000-0003-3922-4581

Notes

The authors declare no competing financial interest.

ACKNOWLEDGMENT

This work was supported by JSPS Grant-in-Aid for Scientific Research (A) [No. 22H00296], JST-CREST [No. JPMJCR22L2], JST-FOREST [No. JPMJFR221U], Grant-in-Aid for JSPS Fellows [No. 23KJ1003], and Joint Research by the National Institutes of Natural Sciences (NINS) [No. 01112104]. This work was also partially supported by Demonstration Project of Innovative Catalyst Technology for Decarbonization through Regional Resource Recycling, the Ministry of the Environment, Government of Japan. We express gratitude to Takuro Kikuchi and Tomonori Toyoda at the Equipment Development Center of the Institute for Molecular Science for their assistance in developing the experimental system, Tomoko Mori at Trans-Omics Facility, NIBB Trans-Scale Biology Center for technical support, and Shota Takahashi and Atsunori Sakurai for their insightful comments on this work. We also acknowledge Mitsuaki Maruoka, Kazuya Watanabe, and Yoshiyasu

Matsumoto for valuable discussions and contributions in the early stage of this research.

REFERENCES

(1) Wang, Q.; Domen, K. Particulate Photocatalysts for Light-Driven Water Splitting: Mechanisms, Challenges, and Design Strategies. *Chem. Rev.* **2020**, *120* (2), 919–985. https://doi.org/10.1021/acs.chemrev.9b00201.

(2) Chen, X.; Shen, S.; Guo, L.; Mao, S. S. Semiconductor-based Photocatalytic Hydrogen Generation. *Chem. Rev.* **2010**, *110* (11), 6503–6570. https://doi.org/10.1021/cr1001645.

(3) Kudo, A.; Miseki, Y. Heterogeneous Photocatalyst Materials for Water Splitting. *Chem. Soc. Rev.* **2009**, *38* (1), 253–278. https://doi.org/10.1039/b800489g.

(4) Huerta-Flores, A. M.; Ruiz-Zepeda, F.; Eyovge, C.; Winczewski, J. P.; Vandichel, M.; Gaberšček, M.; Boscher, N. D.; Gardeniers, H. J. G. E.; Torres-Martínez, L. M.; Susarrey-Arce, A. Enhanced Photocatalytic Hydrogen Evolution from Water Splitting on $Ta_2O_5/SrZrO_3$ Heterostructures Decorated with Cu_xO/RuO_2 Cocatalysts. *ACS Appl. Mater. Interfaces* **2022**, *14* (28), 31767–31781. https://doi.org/10.1021/acsami.2c02520.

(5) Takata, T.; Jiang, J.; Sakata, Y.; Nakabayashi, M.; Shibata, N.; Nandal, V.; Seki, K.; Hisatomi, T.; Domen, K. Photocatalytic Water Splitting with a Quantum Efficiency of Almost Unity. *Nature* **2020**, *581*, 411–414. https://doi.org/10.1038/s41586-020-2278-9.

(6) Chen, Z.; Zhang, Q.; Luo, Y. Experimental Identification of Ultrafast Reverse Hole Transfer at the Interface of the Photoexcited Methanol/Graphitic Carbon Nitride System. *Angew. Chem. Int. Ed.* **2018**, *57* (19), 5320–5324. https://doi.org/10.1002/anie.201713102.

(7) Yamauchi, M.; Saito, H.; Sugimoto, T.; Mori, S.; Saito, S. Sustainable Organic Synthesis Promoted on Titanium Dioxide Using Coordinated Water and Renewable Energies/Resources. *Coord. Chem. Rev.* **2022**, *472*, 214773. https://doi.org/10.1016/j.ccr.2022.214773.

(8) Liu, F.; Feng, N.; Wang, Q.; Xu, J.; Qi, G.; Wang, C.; Deng, F. Transfer Channel of Photoinduced Holes on a TiO_2 Surface as Revealed by Solid-State Nuclear Magnetic Resonance and Electron Spin Resonance Spectroscopy. *J. Am. Chem. Soc.* **2017**, *139* (29), 10020–10028. https://doi.org/10.1021/jacs.7b04877.

(9) Yang, L.; Feng, N.; Wang, Q.; Chu, Y.; Xu, J.; Deng, F. Surface Water Loading on Titanium Dioxide Modulates Photocatalytic Water Splitting. *Cell Reports Phys. Sci.* **2020**, *1* (2), 100013. https://doi.org/10.1016/j.xcrp.2019.100013.

(10) Wang, D.; Sheng, T.; Chen, J.; Wang, H.; Hu, P. Identifying the Key Obstacle in Photocatalytic Oxygen Evolution on Rutile TiO_2. *Nat. Catal.* **2018**, *1*. 291–299. https://doi.org/10.1038/s41929-018-0055-z.

(11) Shirai, K.; Sugimoto, T.; Watanabe, K.; Haruta, M.; Kurata, H.; Matsumoto, Y. Effect of Water Adsorption on Carrier Trapping Dynamics at the Surface of Anatase TiO_2 Nanoparticles. *Nano Lett.* **2016**, *16* (2), 1323–1327. https://doi.org/10.1021/acs.nanolett.5b04724.

(12) Shirai, K.; Fazio, G.; Sugimoto, T.; Selli, D.; Ferraro, L.; Watanabe, K.; Haruta, M.; Ohtani, B.; Kurata, H.; Valentin, C. D.; Matsumoto, Y. Water-Assisted Hole Trapping at the Highly Curved Surface of Nano-TiO_2 Photocatalyst. *J. Am. Chem. Soc.* **2018**, *140* (4), 1415–1422. https://doi.org/10.1021/jacs.7b11061.

(13) He, Y.; Tilocca, A.; Dulub, O.; Selloni, A.; Diebold, U. Local Ordering and Electronic Signatures of Submonolayer Water on Anatase TiO_2(101). *Nat. Mater.* **2009**, *8*, 585–589. https://doi.org/10.1038/nmat2466.

(14) Zhao, Z.; Li, Z.; Zou, Z. Structure and Properties of Water on the Anatase TiO_2(101) Surface: From Single-Molecule Adsorption to Interface Formation. *J. Phys. Chem. C* **2012**, *116* (20), 11054–11061. https://doi.org/10.1021/jp301468c.

(15) Soria, F. A.; Valentin, C. D. Reactive Molecular Dynamics Simulations of Hydration Shells Surrounding Spherical TiO_2 Nanoparticles: Implications for Proton-Transfer Reactions. *Nanoscale* **2021**, *13* (7), 4151–4166. https://doi.org/10.1039/donr07503e.

(16) Fazio, G.; Selli, D.; Ferraro, L.; Seifert, G.; Valentin, C. D. Curved TiO_2 Nanoparticles in Water: Short (Chemical) and Long (Physical) Range Interfacial Effects. *ACS Appl. Mater. Interfaces* **2018**, *10* (35), 29943–29953. https://doi.org/10.1021/acsami.8b08172.

(17) Tan, S.; Feng, H.; Zheng, Q.; Cui, X.; Zhao, J.; Luo, Y.; Yang, J.; Wang, B.; Hou, J. G. Interfacial Hydrogen-Bonding Dynamics in Surface-Facilitated Dehydrogenation of Water on TiO_2(110). *J. Am. Chem. Soc.* **2020**, 142(2), 826–834. https://doi.org/10.1021/jacs.9b09132.

(18) Ma, X.; Shi, Y.; Liu, J.; Li, X.; Cui, X.; Tan, S.; Zhao, J.; Wang, B. Hydrogen-Bond Network Promotes Water Splitting on the TiO_2 Surface. *J. Am. Chem. Soc.* **2022**, *144* (30), 13565–13573. https://doi.org/10.1021/jacs.2c03690.

(19) Yang, W.; Wei, D.; Jin, X.; Xu, C.; Geng, Z.; Guo, Q.; Ma, Z.; Dai, D.; Fan, H.; Yang, X. Effect of the Hydrogen Bond in Photoinduced Water Dissociation: A Double-Edged Sword. *J. Phys. Chem. Lett.* **2016**, *7* (4), 603–608. https://doi.org/10.1021/acs.jpclett.6b00015.

(20) Wagstaffe, M.; Dominguez-Castro, A.; Wenthaus, L.; Palutke, S.; Kutnyakhov, D.; Heber, M.; Pressacco, F.; Dziarzhytski, S.; Gleißner, H.; Gupta, V. K.; Redlin, H.; Dominguez, A.; Frauenheim, T.; Rubio, A.; Stierle, A.; Noei, H. Photoinduced Dynamics at the Water/TiO_2(101) Interface. *Phys. Rev. Lett.* **2023**, *130* (10), 108001. https://doi.org/10.1103/physrevlett.130.108001.

(21) Bakker, H. J.; Skinner, J. L. Vibrational Spectroscopy as a Probe of Structure and Dynamics in Liquid Water. *Chem. Rev.* **2010**, *110* (3), 1498–1517. https://doi.org/10.1021/cr9001879.

(22) Perakis, F.; Marco, L. D.; Shalit, A.; Tang, F.; Kann, Z. R.; Kühne, T. D.; Torre, R.; Bonn, M.; Nagata, Y. Vibrational Spectroscopy and Dynamics of Water. *Chem. Rev.* **2016**, 116 (13), 7590–7607. https://doi.org/10.1021/acs.chemrev.5b00640.

(23) Yoshida, H.; Yamada, R.; Yoshida, T. Platinum Cocatalyst Loaded on Calcium Titanate Photocatalyst for Water Splitting in a Flow of Water Vapor. *ChemSusChem* **2019**, *12* (9), 1958–1965. https://doi.org/10.1002/cssc.201802799.

(24) Matsubara, K.; Inoue, M.; Hagiwara, H.; Abe, T. Photocatalytic Water Splitting over Pt-Loaded TiO_2 (Pt/TiO_2) Catalysts Prepared by the Polygonal Barrel-Sputtering Method. *Appl. Catal. B Environ.* **2019**, *254*, 7–14. https://doi.org/10.1016/j.apcatb.2019.04.075.

(25) Yamaguti, K.; Sato, S. Photolysis of Water over Metallized Powdered Titanium Dioxide. *J. Chem. Soc. Faraday Trans. 1.* **1985**, *81* (5), 1237–1246. https://doi.org/10.1039/F19858101237.

(26) Sheng, H.; Zhang, H.; Song, W.; Ji, H.; Ma, W.; Chen, C.; Zhao, J. Activation of Water in Titanium Dioxide Photocatalysis by Formation of Surface Hydrogen Bonds: An in Situ IR Spectroscopy Study. *Angew. Chem. Int. Ed.* **2015**, *54* (20), 5905–5909. https://doi.org/10.1002/anie.201412035.

(27) Liu, T.; Pan, Z.; Vequizo, J. J. M.; Kato, K.; Wu, B.; Yamakata, A.; Katayama, K.; Chen, B.; Chu, C.; Domen, K. Overall Photosynthesis of H_2O_2 by an Inorganic Semiconductor. *Nat. Commun.* **2022**, *13*, 1–8. https://doi.org/10.1038/s41467-022-28686-x.

(28) Yu, F. Y.; Zhou, Y. J.; Tan, H. Q.; Li, Y. G.; Kang, Z. H. Versatile Photoelectrocatalysis Strategy Raising Up the Green Production of Hydrogen Peroxide. *Adv. Energy Mater.* **2023**, *13* (14), 2300119. https://doi.org/10.1002/aenm.202300119.

(29) Liu, J.; Zou, Y.; Jin, B.; Zhang, K.; Park, J. H. Hydrogen Peroxide Production from Solar Water Oxidation. *ACS Energy Lett.* **2019**, *4* (12), 3018–3027. https://doi.org/10.1021/acsenergylett.9b02199.

(30) Dionigi, F.; Vesborg, P. C. K.; Pedersen, T.; Hansen, O.; Dahl, S.; Xiong, A.; Maeda, K.; Domen, K.; Chorkendorff, I. Gas Phase Photocatalytic Water Splitting with $Rh_{2-y}Cr_yO_3$/GaN:ZnO in

μ-Reactors. *Energy Environ. Sci.* **2011**, *4* (8), 2937–2942. https://doi.org/10.1039/c1ee01242h.

(31) Suguro, T.; Kishimoto, F.; Kariya, N.; Fukui, T.; Nakabayashi, M.; Shibata, N.; Takata, T.; Domen, K.; Takanabe, K. A Hygroscopic Nano-Membrane Coating Achieves Efficient Vapor-Fed Photocatalytic Water Splitting. *Nat. Commun.* **2022**, *13*, *5698*. https://doi.org/10.1038/s41467-022-33439-x.

(32) Amano, F.; Ishikawa, A.; Sato, H.; Akamoto, C.; Singh, S. P.; Yamazoe, S.; Sugimoto, T. Facilitating Methane Conversion and Hydrogen Evolution on Platinized Gallium Oxide Photocatalyst through Liquid-like Water Nanofilm Formation. *Catal. Today* **2024**, *426* (15), 114375. https://doi.org/10.1016/j.cattod.2023.114375.

(33) Klug, D. D.; Mishima, O.; Whalley, E. High-Density Amorphous Ice. IV. Raman Spectrum of the Uncoupled O–H and O–D Oscillators. *J. Chem. Phys.* **1987**, *86* (10), 5323–5328. https://doi.org/10.1063/1.452557.

(34) Sugimoto, T.; Matsumoto, Y. Orientational Ordering in Heteroepitaxial Water Ice on Metal Surfaces. *Phys. Chem. Chem. Phys.* **2020**, *22* (29), 16453–16466. https://doi.org/10.1039/docp01763a.

(35) Auer, B. M.; Skinner, J. L. IR and Raman Spectra of Liquid Water: Theory and Interpretation. *J. Chem. Phys.* **2008**, *128* (22), 224511. https://doi.org/10.1063/1.2925258.

(36) Verdaguer, A.; Weis, C.; Oncins, G.; Ketteler, G.; Bluhm, H.; Salmero, M. Growth and Structure of Water on SiO_2 Films on Si Investigated by Kelvin Probe Microscopy and in Situ X-Ray Spectroscopies. *Langmuir* **2007**, *23* (19), 9699–9703. https://doi.org/10.1021/la700893w.

(37) Orlando, F.; Artiglia, L.; Yang, H.; Kong, X.; Roy, K.; Waldner, A.; Chen, S.; Bartels-Rausch, T.; Ammann, M. Disordered Adsorbed Water Layers on TiO_2 Nanoparticles under Subsaturated Humidity Conditions at 235 K. *J. Phys. Chem. Lett.* **2019**, *10* (23), 7433–7438. https://doi.org/10.1021/acs.jpclett.9b02779.

(38) Sang, L.; Zhang, Y.; Wang, J.; Zhao, Y.; Chen, Y. T. Correlation of the Depletion Layer with the Helmholtz Layer in the Anatase TiO_2-H_2O Interface Via Molecular Dynamics Simulations. *Phys. Chem. Chem. Phys.* **2016**, *18* (22), 15427–15435. https://doi.org/10.1039/c6cp01990k.

(39) Ohno, K.; Okimura, M.; Akai, N.; Katsumoto, Y. The Effect of Cooperative Hydrogen Bonding on the OH Stretching-Band Shift for Water Clusters Studied by Matrix-Isolation Infrared Spectroscopy and Density Functional Theory. *Phys. Chem. Chem. Phys.* **2005**, *7* (16), 3005–3014. https://doi.org/10.1039/b506641g.

(40) Tao, Y.; Zou, W.; Kraka, E. Strengthening of Hydrogen Bonding with the Push-Pull Effect. *Chem. Phys. Lett.* **2017**, *685*, 251–258. https://doi.org/10.1016/j.cplett.2017.07.065.

(41) Liu, L. M.; Zhang, C.; Thornton, G.; Michaelides, A. Structure and Dynamics of Liquid Water on Rutile TiO_2 (110). *Phys. Rev. B* **2010**, *82* (16), 161415. https://doi.org/10.1103/PhysRevB.82.161415.

(42) Chen, J.; Li, Y. F.; Sit, P.; Selloni, A. Chemical Dynamics of the First Proton-Coupled Electron Transfer of Water Oxidation on TiO_2 Anatase. *J. Am. Chem. Soc.* **2013**, *135* (50), 18774–18777. https://doi.org/10.1021/ja410685m.

(43) Andrade, M. F. C.; Ko, H. Y.; Zhang, L.; Car, R.; Selloni, A. Free Energy of Proton Transfer at the Water-TiO_2 Interface from Ab Initio Deep Potential Molecular Dynamics. *Chem. Sci.* **2020**, *11* (9), 2335–2341. https://doi.org/10.1039/c9sc05116c.

(44) Ma, H.; Feng, J.; Jin, F.; Wei, M.; Liu, C.; Ma, Y. Where Do Photogenerated Holes at the g-C_3N_4/Water Interface Go for Water Splitting: H_2O or OH^-? *Nanoscale* **2018**, *10* (33), 15624–15631. https://doi.org/10.1039/c8nr04505d.

(45) Cheng, J.; Vandevondele, J.; Sprik, M. Identifying Trapped Electronic Holes at the Aqueous TiO_2 Interface. *J. Phys. Chem. C* **2014**, *118* (10), 5437–5444. https://doi.org/10.1021/jp5007694q.

(46) Ding, Z.; Goldsmith, Z. K.; Selloni, A. Pathways for Electron Transfer at MgO-Water Interfaces from Ab Initio Molecular Dynamics. *J. Am. Chem. Soc.* **2022**, *144* (4), 2002–2009. https://doi.org/10.1021/jacs.1c13250.

(47) Wood, B. C.; Schwegler, E.; Choi, W. I.; Ogitsu, T. Hydrogen-Bond Dynamics of Water at the Interface with InP/GaP(001) and the Implications for Photoelectrochemistry. *J. Am. Chem. Soc.* **2013**, 135 (42), 15774–15783. https://doi.org/10.1021/ja403850s.

(48) Ledezma-Yanez, I.; Wallace, W. D. Z.; Sebastián-Pascual, P.; Climent, V.; Feliu, J. M.; Koper, M. T. M. Interfacial Water Reorganization as a pH-Dependent Descriptor of the Hydrogen Evolution Rate on Platinum Electrodes. *Nat. Energy* **2017**, *2*, 1–7. https://doi.org/10.1038/nenergy.2017.31.

(49) Pecina, O.; Schmickler, W. A Model for Electrochemical Proton-Transfer Reactions. *Chem. Phys.* **1998**, *228* (1), 265–277. https://doi.org/https://doi.org/10.1016/S0301-0104(97)00299-1.

(50) Wang, Q.; Lian, J.; Bai, Y.; Hui, J.; Zhong, J.; Li, J.; An, N.; Yu, J.; Wang, F. Photocatalytic Activity of Hydrogen Production from Water over TiO_2 with Different Crystal Structures. *Mater. Sci. Semicond. Process.* **2015**, *40*, 418–423. https://doi.org/10.1016/j.mssp.2015.06.089.

(51) Vequizo, J. J. M.; Matsunaga, H.; Ishiku, T.; Kamimura, S.; Ohno, T.; Yamakata, A. Trapping-Induced Enhancement of Photocatalytic Activity on Brookite TiO_2 Powders: Comparison with Anatase and Rutile TiO_2 Powders. *ACS Catal.* **2017**, *7* (4), 2644–2651. https://doi.org/10.1021/acscatal.7b00131.

(52) Bai, S.; Wang, L.; Li, Z.; Xiong, Y. Facet-Engineered Surface and Interface Design of Photocatalytic Materials. *Adv. Sci.* **2017**, *4* (1), 1600216. https://doi.org/10.1002/advs.201600216.

Authors are required to submit a graphic entry for the Table of Contents (TOC) that, in conjunction with the manuscript title, should give the reader a representative idea of one of the following: A key structure, reaction, equation, concept, or theorem, etc., that is discussed in the manuscript. Consult the journal's Instructions for Authors for TOC graphic specifications.

Insert Table of Contents artwork here